AD-A122 786 ACTA ARMAMENTARII (SELECTED ARTICLES)(U) FOREIGN TECHNOLOGY DIV WRIGHT-PATTERSON AFB OH J LUO ET AL. 01 DEC 82 FTD-ID(RS)T-0801-82 1/1

UNCLASSIFIED F/G 21/9.2 NL

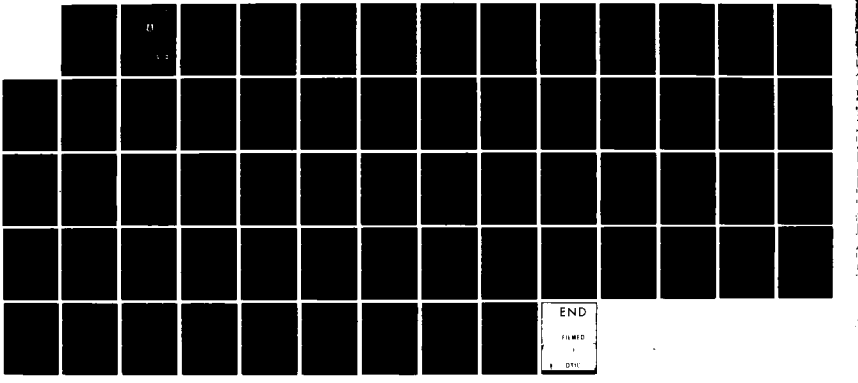

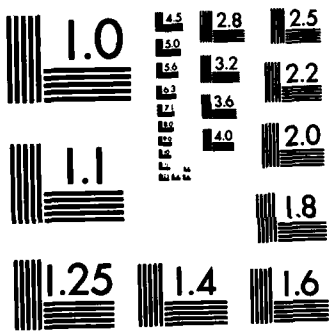

FTD-ID(RS)T-0801-82

AD A122786

FOREIGN TECHNOLOGY DIVISION

ACTA ARMAMENTARII

(Selected Articles)

DTIC
ELECTE
DEC 29 1982
S D
D

Approved for public release;
distribution unlimited.

DTIC FILE COPY

82 12 28 183

EDITED TRANSLATION

FTD-ID(RS)T-0801-82 1 December 1982

MICROFICHE NR: FTD-82-C-001537

ACTA ARMAMENTARII (Selected Articles)

English pages: 59

Source: Binggong Xuebao, Nr. 1, February 1982, pp. 1-9; 38-57

Country of origin: China
Translated by: LEO KANNER ASSOCIATES
F33657-81-D-0264
Requester: FTD/TQTA

PREPARED BY:

TRANSLATION DIVISION
FOREIGN TECHNOLOGY DIVISION
WP-AFB, OHIO.

CONTENTS

GRAPHICS DISCLAIMER

All figures, graphics, tables, equations, etc. merged into this translation were extracted from the best quality copy available.

A STUDY OF THE MAXIMUM SOLID ROCKET ENGINE THRUST NOZZLE SURFACE FOR ONE-DIMENSIONAL TWO-PHASE FLOWS

by Luo Junyang and Sun Yue

Abstract

This paper uses the Pontryagin Maximum Principle to study the problem of the optimal nozzle surface for one-dimensional two-phase flows. Choosing the slope as the control variable, we verified that the optimal surface was a conical surface composed of a group of straight lines with the slope being constant. Furthermore, we discussed the method of defining the optimal contour in the subsonic and supersonic regions. This paper can provide a theoretical basis and computation reference for the design of nozzles.

Basic Symbols

p = pressure
u = speed
T = temperature
G = weight flow volume
k_g = gas-specific heat ratio
C_{pg}, C_{pl} = gas, particle specific heat
g = gravitational acceleration
x = x direction coordinate
y = radius of corresponding independent variable x
M_p = Al_2O_3 material density
R_g = gas constant
A_Q = mechanical equivalent of heat
g' = heat transfer correction coefficient
f' = drag correction coefficient
μ_g = gas kinematic viscosity coefficient
Pr = Prandtl number
r_p = particle radius

α = interval of convergence half angle
β = diffusion region half angle
p_a = external atmospheric pressure

Lower Symbols

g = gas phase
p = particle phase

I. Preface

Early, in 1963, F.E. Marble [1] used the one-dimensional flow minimum hysteresis method for the design of the optimal nozzle surface for two-phase flows. He only attained an integral expression but this method is not appropriate in engineering technology. In 1968, A.N. Krayko, V.K. Starkov and L.Ye. Sternin [2] used the supposition of the one-dimensional flow and employed the calculus of variations to compute seven maximum thrust nozzles in the supersonic region by means of an electronic computer. Its surface is a linear region yet this method cannot use an analytical solution to verify the optimal nozzle surface. From 1966 to 1972, Hoffman et al [3] used the two-dimensional flow theory and the calculus of variations to compute the optimal nozzle surface in the supersonic region. Because at present there is still no perfect method for the flow of the two-dimensional subsonic and supersonic regions in two-phase flows, difficulties occur even if this method is practically applied.

This paper investigates the problem of the optimal rocket engine surface for one-dimensional two-phase flows using the maximum principle to find the best system of solutions. If the boundary conditions are given, we can find the corresponding optimal nozzle contour lines.

II. Basic Theories and Hypotheses

1. Based on reference materials [4], there are the

following hypotheses:

a. The flow is one-dimensional and stable;

b. The system exchanges with the external non-thermal quantity and the mass;

c. Aside from the drag effect produced on the particle, the gas is considered non-viscous;

d. The energy exchange between the gas and particles is only limited to the convection heat transfer;

e. The gas flow is the condensed flow of an ideal gas and the Al_2O_3 particles take on a liquid state (if below the solid point, it also assumes a supercooling liquid state);

f. The shape of the particles is circular;

g. The internal temperature of the particles is uniform;

h. The Brownian motion does not affect the pressure;

i. The area occupied by the particles can be neglected;

j. There is no collision between the particles and the diameters of the particles do not change during the flow process.

2. Basic Theories

Based on the maximum principle of P.S. Pontryagin [5], we used the Lagrange optimum performance index functional form of

$$J = \int_{x_0}^{x_f} \phi(u, w, x)dx \qquad (1)$$

(1) Equation of state

$$\frac{\partial H}{\partial \lambda} = \dot{u} = f(u, w, x) \qquad (2)$$

In the equation: $u^T = (u_1, u_2, \cdots\cdots, u_n)$ is the state variable and $w^T = (w_1, w_2, \cdots\cdots, w_n)$ is the control variable.

(2) Conjugate equation

$$\frac{\partial H}{\partial u} = -\dot{\lambda} = \frac{\partial f^T[u(x), w(x), x]}{\partial u}\lambda(x) + \frac{\partial \phi[u(x), w(x), x]}{\partial u} \qquad (3)$$

(3) H function

$$H=\phi[u(x),\ w(x),\ x]+\lambda^{T}(x)f\ [u(x),\ w(x),\ x] \qquad (4)$$

(4) Optimum principle

If w is one inner point of $\mathcal{W}$, then we have

$$\frac{\partial H}{\partial w}=0 \qquad (5)$$

If $\omega \in \mathcal{W}$ is an arbitrary point, then $\frac{\partial H}{\partial \omega}$ possibly does not exist. If we let H be the minimum (maximum) control $\hat{\omega}$, and the arbitrary adjacent control is ω , then

$$H(u,\ \hat{w},\ \lambda,\ x)=\min_{w\in w} H(u,\ w,\ \lambda,\ x)$$

or

$$H(u,\ \hat{w},\ \lambda,\ x)=\max_{w\in w} H(u,\ w,\ \lambda,\ x) \qquad (6)$$

(5) Transverse conditions

The transverse conditions are not sufficient to compensate for the boundary conditions. The end point free transverse conditions are

$$\left.\begin{aligned} &\lambda(x_f)=\left(\frac{\partial\theta}{\partial u}\right)_{x_f}+\left(\frac{\partial N^{T}}{\partial u}\right)_{x_f}\nu \\ &N\ [u(x_f),x_f]=0 \\ &H[u(x_f),\ w(x_f),\ \lambda(x_f),x_f]+\frac{\partial\theta}{\partial x_f}+\frac{\partial N^{T}}{\partial x_f}\nu=0 \end{aligned}\right\} \qquad (7)$$

In the equation: N $[u(x_f), x_f]$ is the flow equation and v is the multiplier.

Equation (7) is a two point limit value problem which requires the use of the iteration method to find its numerical solution. This is naturally very difficult. Yet, for one-dimensional two-phase flow engines, the equation of state and value functional both have specific forms, that is, contain the linear item of slope $\dot{y}$. This allows us to possibly use the Pontryagin Maximum Principle to find the theoretically optimal nozzle surface.

III. Equations of State

Based on the above assumptions, we can obtain:

1. The gas motion equations

$$\rho_g u_g \frac{du_g}{dx} + \frac{dp_g}{dx} = -A\rho_p(u_g - u_p) \tag{8}$$

$$\frac{1}{p_g}\frac{dp_g}{dx} - \frac{k_g d\rho_g}{\rho_g dx} = \frac{A\rho_p B}{p_g u_g} \tag{9}$$

In the equations

$$B = (k_g - 1)\left[(u_g - u_p)^2 + \frac{2}{3}\frac{g}{A_Q}C(T_p - T_g)\right]$$

$$A = \frac{9}{2}\frac{f'\mu_g}{M_g r_p^2}$$

$$C = \frac{g'}{f'}\frac{C_{p_g}}{\mathrm{Pr}}$$

$$G_g = g\rho_g u_g \pi y^2 \tag{10}$$

2. Particle motion equations

$$\frac{du_p}{dx} = A\frac{(u_g - u_p)}{u_p} \tag{11}$$

$$\frac{dT_p}{dx} = -\frac{2}{3}\frac{AC}{C_{p_1}}\frac{(T_p - T_g)}{u_p} \tag{12}$$

$$G_p = g\rho_p u_p \pi y^2 \tag{13}$$

After equations (8) to (13) undergo mathematical processing, they can finally change into

$$\frac{du_g}{dx} = \left[\frac{\pi y^2 u_g g}{G_g u_g - k_g \pi y^2 p_g g}\right]\left\{\frac{2k_g p_g}{y}\dot{y} + A\frac{G_p}{g\pi y^2 u_p}(u_p - u_g)\right.$$
$$\left. - \frac{AG_p(k_g - 1)}{g\pi y^2 u_p u_g}(u_g - u_p)^2 - \frac{2}{3}\frac{ACG_p}{A_0 \pi y^2 u_p u_g}(k_g - 1)\left(T_p - \frac{p_g \pi y^2 u_g}{R_g G_g}\right)\right\} \tag{14}$$

Letting

$$v_1 = \frac{g\pi y^2 u_g}{G_g u_g - k_g \pi y^2 p_g g}$$

$$v_2 = \frac{2k_g p_g}{y}\dot{y}$$

$$v_3 = A\frac{G_p}{g\pi y^2 u_p}(u_p - u_g)$$

$$v_4 = \frac{AG_p(k_g - 1)}{g\pi y^2 u_p u_g}(u_g - u_p)^2$$

$$v_5 = \frac{2}{3}\frac{ACG_p}{A_0 \pi y^2 u_p u_g}(k_g - 1)$$

$$v_6 = \left(T_p - \frac{p_g \pi y^2 u_g}{R_g G_g}\right)$$

We finally obtain

$$\frac{du_g}{dx} = v_1(v_2 + v_3 - v_4 - v_5 v_6) = \mathcal{U} \tag{15}$$

From equations (15) and (8) we can solve

$$\frac{dp_g}{dx} = -\frac{G_g}{g\pi y^2}\left[-\frac{G_p}{G_g} A \frac{u_g - u_p}{u_p} + \mathcal{U}\right] \tag{16}$$

From equation (12) it can change into

$$\frac{dT_p}{dx} = -\frac{2}{3}\frac{ACv_g}{C_{p_1} u_p} \tag{17}$$

When equations (11), (15), (16) and (17) are equations of state for two-phase flows, they can be written as general forms

$$\frac{du_g}{dx} = f_1(u_g, p_g, u_p, T_p, y, \dot{y}) = f_1(u, \dot{y})$$

$$\frac{dp_g}{dx} = f_2(u_g, p_g, u_p, T_p, y, \dot{y}) = f_2(u, \dot{y})$$

$$\frac{du_p}{dx} = f_3(u_g, u_p) = f_3(u)$$

$$\frac{dT_p}{dx} = f_4(u_g, p_g, u_p, T_p, y) = f_4(u)$$

We can see from the four equations of state above that aside from containing five state variables, $u^T=(u_g, p_g, u_p, T_p, y)$, they also contain a derivative of a state variable. In $\dot{y}=\frac{dy}{dx}$, $\dot{y}$ is selected as the control variable. Therefore, there are five equations of state altogether.

IV. Value Functional

Because the nozzle is composed of the convergence and expansion regions as shown in fig. 1, the value functional is

$$J=\int_{x_0}^{x_f}2\pi(p_g-p_a)y\dot{y}dx$$

$$=\int_{x_0}^{x_1}2\pi(p_g-p_a)y\dot{y}dx+\int_{x_1}^{x_f}2\pi(p_g-p_a)y\dot{y}dx \tag{18}$$

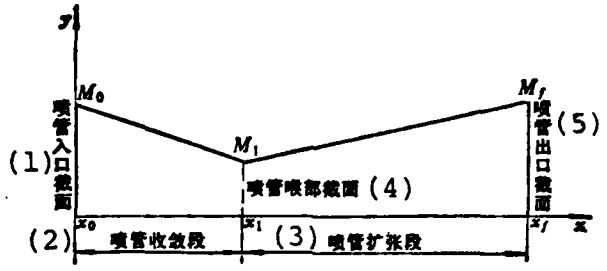

Fig. 1 Diagram of Nozzle Surface

Key: 1. Nozzle inlet section
2. Nozzle convergence region
3. Nozzle expansion region
4. Nozzle throat section
5. Nozzle outlet section

V. The Hamilton Function

Two end points are given wherein the terminal end point can be stable as well as free. When there are no other constraining conditions, the H function can be written as

$$H=\lambda_{a_g}\mathcal{U}+\lambda_{a_p}A\frac{u_g-u_p}{u_p}-\lambda_{p_g}\frac{G_g}{\pi y^2 g}\left[A\frac{G_p}{G_g u_p}(u_g-u_p)+\mathcal{U}\right]$$

$$-\frac{2}{3}\lambda_{T_p}\frac{ACv_g}{C_{p_1}u_p}+\lambda_y\dot{y}+2\pi(p_g-p_a)y\dot{y} \tag{19}$$

Equation (19) is the H function when there are no constraining conditions. Its general form is

$$H=\phi(u)\dot{y}+\lambda^{T}f(u,\dot{y})$$

V1. The Conjugate Equation

When we use the H function to find the negative partial derivative of the state variable, we obtain a conjugate equation

$$\frac{d\lambda_{ag}}{dx}=\lambda_{pg}\frac{G_pA}{g\pi y^2u_p}-\frac{\partial\mathcal{U}}{\partial u_g}\left(\lambda_{ag}-\lambda_{pg}\frac{G_g}{g\pi y^2}\right)-\lambda_{ap}\frac{A}{u_p}-\frac{2}{3}\lambda_{Tp}\frac{ACh_3}{C_{pl}u_p} \quad (20)$$

In the equation

$$\frac{\partial\mathcal{U}}{\partial u_g}=v_1\left[(v_2+v_3-v_4-v_5v_6)\left(\frac{1}{u_g}-v_1h_1\right)+\left(v_5h_3-h_2-\frac{2v_4}{(u_g-u_p)}+\frac{v_4}{u_g}+v_6\frac{v_5}{u_g}\right)\right]$$

$$h_1=\frac{G_g}{g\pi y^2u_g}$$

$$h_2=A\frac{G_p}{g\pi y^2u_p}$$

$$h_3=\frac{p_g\pi y^2}{R_gG_g}$$

Equation (20) is written as the general forms

$$\frac{d\lambda_{ag}}{dx}=g_1(u,\lambda)+h_1(u,\lambda,\dot{y})$$

$$\frac{d\lambda_{pg}}{dx}=-\frac{\partial\mathcal{U}}{\partial p_g}\left(\lambda_{ag}-\lambda_{pg}\frac{G_g}{g\pi y^2}\right)-2\pi y\dot{y}-\frac{2}{3}\lambda_{Tp}\frac{AC}{C_{pl}u_pgR_gh_1} \quad (21)$$

In the equation

$$\frac{\partial\mathcal{U}}{\partial p_g}=v_1^2\frac{K_g}{u_g}(v_2+v_3-v_4-v_5v_6)+\left(2K_g\frac{\dot{y}}{y}+v_5\frac{1}{gR_gh_1}\right)v_1$$

Equation (21) is written as the general form

$$\frac{d\lambda_{pg}}{dx} = g_2(u, \lambda) + h_2(u, \lambda, \dot{y})$$

$$\frac{d\lambda_{up}}{dx} = -\frac{\partial \mathcal{U}}{\partial u_p}\left(\lambda_{ug} - \lambda_{pg}\frac{G_g}{g\pi y^2}\right) - \left(\lambda_{pg}\frac{AG_p}{g\pi y^2} - A\lambda_{up}\right)\frac{u_g}{u_p^2}$$

$$-\frac{2}{3}\lambda_{Tp}\frac{ACv_g}{C_{p_i}u_p^2} \qquad (22)$$

Equation (22) is written as the general form

$$\frac{d\lambda_{up}}{dx} = g_3(u, \lambda)$$

$$\frac{d\lambda_{Tp}}{dx} = v_1 v_g\left(\lambda_{ug} - \lambda_{pg}\frac{G_g}{g\pi y^2}\right) + \frac{2}{3}\lambda_{Tp}\frac{AC}{C_{p_i}u_p} \qquad (23)$$

Equation (23) is written as the general form

$$\frac{d\lambda_{Tp}}{dx} = g_4(u, \lambda)$$

$$\frac{d\lambda_y}{dx} = -\frac{\partial \mathcal{U}}{\partial y}\left(\lambda_{ug} - \lambda_{pg}\frac{G_g}{g\pi y^2}\right) - 2\mathcal{U}\frac{G_g\lambda_{pg}}{g\pi y^3} + \frac{2v_3\lambda_{pg}}{y}$$

$$-\frac{4}{3}\lambda_{Tp}\frac{ACp_g\pi y u_g}{C_{p_i}u_p R_g G_g} - 2\pi(p_g - p_a)\dot{y} \qquad (24)$$

In the Equation

$$\frac{\partial \mathcal{U}}{\partial y}=\left(\frac{2v_1}{y}+2K_g p_g \frac{v_1^2}{yu_g}\right)(v_2+v_3-v_4-v_5v_6)+v_1\left(-\frac{2K_g p_g}{y^2}\dot{y}\right.$$
$$\left.-\frac{2v_3}{y}+\frac{2v_4}{y}+v_5\frac{2\pi p_g yu_g}{R_g G_g}+v_6\frac{2v_5}{y}\right)$$

Equation (24) is written as the general form

$$\frac{d\lambda_y}{dx}=g_3(u,\lambda)+h_3(u,\lambda,\dot{y})$$

V11. Defining the Optimal Contour Line

We obtain from the equation of state and proposed value functional equation (18) that the H function is the linear function of $\dot{y}$

$$H=H_1(u,\lambda)+H_2(u,\lambda)\dot{y}$$

If we first consider the subsonic region, our given limit is

$$k_1\leqslant|\dot{y}| \qquad (25)$$

The aim of this article is the design of an optimal surface and therefore $\dot{y}$ acts as the control variable. Based on the maximum principle, we should select control variable $\dot{y}$ so that H function takes on a minimum value. Because of this, control variable $\dot{y}$ should take a numerically allowable minimum value and the symbol should be opposite that of H_2 ($H_2>0$ is equal to the subsonic region, $H_2<0$ is equal to the supersonic region). Then

$$\dot{y}=-k_1 \qquad (26)$$

In this way, we obtained the optimal solution group: i.e. limited the group of straight lines of the slope. It is very noticeable that the obtained maximal solution group can satisfy the boundary conditions of the two points. From equation (26) we can obtain

$$y=-k_1x+c_2$$

k_1 and c_2 are both undetermined constants which can be determined by the two boundary conditions. For example, by means of the two fixed points $M_o(x_o,y_o)$ and $M_1(x_1,y_1)$ or by the $M_o(x_o,y_o)$ point and the convergence region's half angle α.

The first situation is

$$y_1-y_0=-k_1(x_1-x_0)$$

$$k_1=-\frac{y_1-y_0}{x_1-x_0}$$

$$y_0=-k_1x_0+c_2$$

$$c_2=y_0+k_1x_0=y_0-\frac{y_1-y_0}{x_1-x_0}x_0$$

As a result, we fix constants k_1 and c_2.

The second situation is

$$\dot{y}=-k_1=-\mathrm{tg}\,\alpha$$

Then we obtain

$$k_1=\mathrm{tg}\,\alpha$$
$$y_0=-x_0\mathrm{tg}\alpha+c_2$$
$$c_2=y_0+x_0\mathrm{tg}\,\alpha$$

That is, the given boundary conditions can determine a subsonic region maximal contour line.

In the same way, control variable $\dot{y}$ is limited by the following in the supersonic region

$$k_2 \geqslant \dot{y} > 0$$

Then, from the maximum principle we obtain

$$\dot{y} = k_2$$

The maximal solution group is also the slope sustaining the limited group of straight lines. By integration we obtain

$$y = k_2 x + c_2$$

It can also suit the boundary conditions of the two points. As a result, the obtained optimal supersonic region surface is also a group of straight lines. In this way, we can obtain the optimal nozzle surface as shown in fig. 2.

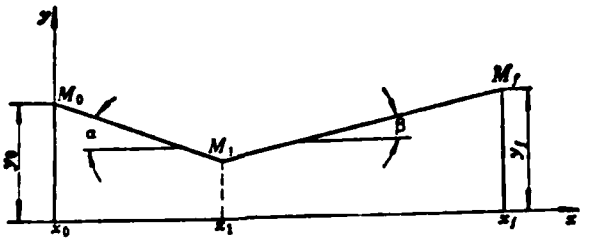

Fig. 2 Chart of the Maximal Nozzle Surface When the Given Boundary Conditions are $y_0 \alpha$ and $y_f \beta$

In the aforementioned value function

$$J = \int_{x_0}^{x_1} 2\pi(p_g - p_a)y\dot{y}dx + \int_{x_1}^{x_2} 2\pi(p_g - p_a)y\dot{y}dx \qquad (18)$$

the first item $\int_{x_0}^{x_1} 2\pi(p_g - p_a)y\dot{y}dx$ is the drag. Based on the maximum principle, the $\dot{y}$ selected in this area is the minimum value and thus the entire drag is minimum; the latter item $\int_{x_1}^{x_f} 2\pi(p_g - p_a)$ is the thrust. Based on the maximum principle, the $\dot{y}$ taken in this region is the maximum value. Thus, maximum thrust is produced in this area and from the sum of the two items we then obtain the maximum thrust surface. The reason we can obtain this result is because the Hamiltonian function H is the $\dot{y}$ linear function. Based on the Pontryagin Maximum Principle, after $\dot{y}$ takes the maximum or the minimum, the value function is also the integration of the thrust and drag and takes the maximum value. This is the physical significance of this paper concerning the optimal surface.

V111. Conclusion

The maximum thrust nozzle surface for one-dimensional two-phase flows is a group of conical surfaces when the slope is limited. If we give the boundary conditions, the optimal nozzle surface is a conical surface. Thus, we obtain a deduction: when designing a one-dimensional two-phase flow nozzle surface, convergence half angle α of the subsonic region should be made as small as possible and expansion half angle β of the supersonic region should be made as large as possible.

References

[1] "Nozzle Contours for Minimum particle-Lag Loss", Marble, F.E. AIAA J., Vol. 1, No. 12, 1963.

[2] A.N. Krayko, L.E. Sternin, V.K. Starkov, "Solution of one-dimensional approximation of a variational problem for constructing a maximum-thrust nozzle with gas and extraneous particle flow," Izvestiya AN SSSR, MZhG, 1968, No. 4.

[3] "Design of Maximum Thrust Nozzle for Gas-Particle Flows". A.A. Elsbernd and J.D. Hoffman, AD-729439, AD-729440.

[4] "One Dimensional Flow of a Gas-particle System", J.R. Kliegel, IAS, Paper, No. 60-5.

[5] "Optimum Systems Control", Sec.4, A.P. Sage, 1968.

[6] Qin Shoukang and Zhang Zhengfang, "Optimum Control," Science Publications, 1979.

ITERATIVE CALCULATION METHOD FOR THE EQUILIBRIUM COMPOSITION OF THE COMBUSTION PRODUCTS OF COMPOSITE PROPELLANTS*

by Wan Junhua

Abstract

This paper presents a simplified calculation method which solves the equilibrium composition of the combustion products of composite propellants. Using element mass conservation equations and equilibrium equations for chemical reactions, this paper gives the iterative calculation formulae for calculating the partial pressure of the gas composition. The calculation procedure is simple, clear and much easier for calculating than the concentration method. The calculation results are very close to those obtained by the concentration method, the partial pressure convergence of the composition is very good and to calculate 4 times is generally very accurate. This proved that the simplified calculation method proposed in this paper is reliable.

Main Symbols

A,B,C,D,E,F,L	calculation factors
G	weight or weight fraction of element
K	partial pressure equilibrium constant
m	gram molecular weight of composition
M	weight of composition
n	gram molecular number of composition
pi	partial pressure (atm) of i type
p_Σ	total pressure (atm) of combustion products
Q,R,S,U,V	component constants of propellants
Y	weight fraction or weight of combustion products
Z	gram atomic number of element in propellant
α, β, γ	constant factors
$C_p, H_p, O_p, N_p, Cl_p, S_p$	element weight component of propellant
Φ, χ, Ψ	calculation factors

*Received Dec. 29, 1979.

I. Preface

There are various different methods to calculate the equilibrium composition of the combustion products of propellants, for example, the Huff, White, Brinkley and simplified methods etc. The three aforementioned methods consider the possibly produced combustion products composition. Because the unknown numbers are numerous and calculation is complex, it is generally necessary to use an electronic computer for completion. However, the simplified method overlooks the small quantity composition contained in the combustion products so that calculations are greatly simplified and common calculation tools can be used for completion.

This paper carries out investigations on calculation methods for the equilibrium compositions of combustion products of propellants with 9 elements: C,H,O,N,Cl,S,Al,Cr and Cu. The combustion products of these types of propellants contain a gas phase and condensed phase. After overlooking the very small content of composition, there are three types of condensed phase compositions: Al_2O_3, Cr_2O_3 and Cu. Based on the chemical reaction equations, we used the mass conservation principle to directly find their contents. After using the separation method of independently calculating the condensed phase composition, the unknown number of the gas phase system decreases to 16 types of compositions. The control equations of the partial pressure of the major compositions are still water gas reaction equilibrium equations.

II. Equilibrium Composition Equations

1. The Equilibrium Composition of Combustion Products

Based on materials in the references, the major combustion products gas phase compositions of composite propellants have CO_2, CO, H_2O, H_2, N_2, HCl, SO_2, H_2S, OH, O_2, NO, Cl_2, O, H, N and Cl etc. and the condensed phase compositions have Al_2O_3, Cr_2O_3 and Cu etc. Under high temperatures, the Al_2O_3

separates into Al_2O and AlO. However, because polysulfide propellants do not have very high energy, the temperature of the combustion products is generally about 3,000 K. Under this temperature, the Al_2O_3 is generally not able to separate into Al_2O and AlO.

Hypothesis: all of the sulfur in the propellant participates in the chemical reaction and produces SO_2 and H_2S gas.

Because the sulfur content in composite propellants is not high, generally only about 7%, the oxygen content reaches to over 40%. Moreover, a good deal of H_2 gas can be produced in the combustion products. Sulfur easily oxidizes and produces SO_2. Under high temperatures, the sulfur can also directly combine with hydrogen to produce H_2S gas. Therefore, this hypothesis is close to the actual situation.

Based on the above analysis, for the polysulfide propellant, there are 19 types of equilibrium compositions of this method of calculation: O_2, OH, NO, H_2S, Cl_2, H, Cl, O, N, N_2, SO_2, HCl, CO_2, CO, H_2O, H_2, Al_2O_3, Cr_2O_3 and Cu.

The condensed phase composition is directly solved according to the chemical reaction equations and mass conservation principle. Below we explain by using Al_2O_3 as an example.

Hypothesis: the aluminum and chromium in the propellant is completely oxidized according to the chemical equivalent ratio.

$$2Al + \frac{3}{2}O_2 = Al_2O_3$$
$$53.96 \quad 48 \quad 101.96$$
$$M_{Al} \quad (M_{O_2})_{Al} \quad M_{Al_2O_3}$$

The weight of the produced condensed phase Al_2O_3 is

$$M_{Al_2O_3}=\frac{101.96}{53.96}M_{Al} \quad kg$$

The weight of the consumed oxygen is

$$(M_{O_2})_{Al}=\frac{48}{53.96}M_{Al} \quad kg$$

In the same way, it is easy to find $M_{Cr_2O_s}$ and $(M_{O_2})_{Cr}$.

Therefore, after the combustion of 1 kg of propellant, the produced condensed phase weight (or weight percentage) Y_s and gas phase composition weight Y_g are

$$Y_s=M_{Al_2O_3}+M_{Cr_2O_3}+M_{Cu} \quad kg$$
$$Y_g=1-Y_s \quad kg$$

2. System of Equations for the Equilibrium Composition

The element mass conservation equation: the weight of a certain element in 1 kg of propellant should be equal to the weight of that element in the combustion product. That is

$$C_P=\frac{12Y_g}{\sum m_i p_i}(p_{CO_2}+p_{CO}) \quad (1)$$

$$H_P=\frac{1Y_g}{\sum m_i p_i}(2p_{H_2O}+2p_{H_2}+p_{HCl}+2p_{H_2S}+p_H+p_{OH}) \quad (2)$$

$$O_P=\frac{16Y_g}{\sum m_i p_i}(2p_{O_2}+2p_{CO_2}+p_{CO}+p_{H_2O}+2p_{SO_2}+p_{NO}+p_{OH}+p_O) \quad (3)$$

$$N_P=\frac{14Y_g}{\sum m_i p_i}(2p_{N_2}+p_{NO}+p_N) \quad (4)$$

$$Cl_P=\frac{35.45Y_g}{\sum m_i p_i}(p_{HCl}+2p_{Cl_2}+p_{Cl}) \quad (5)$$

$$S_P=\frac{32Y_g}{\sum m_i p_i}(p_{SO_2}+p_{H_2S}) \quad (6)$$

Because the total weight of the gas phase composition is $Y_g k_g$, the right sides of equations (1)-(6) are all multiplied by factor Y_g.

The dissociation reaction equilibrium equations

$$K_1 = p_{CO} p_{O_2}^{0.5} / p_{CO_2} \quad (7)$$
$$K_2 = p_{H_2} p_{O_2}^{0.5} / p_{H_2O} \quad (8)$$
$$K_3 = p_{CO} p_{H_2O} / p_{CO_2} p_{H_2} \quad (9)$$
$$K_4 = p_{OH} p_{H_2}^{0.5} / p_{H_2O} \quad (10)$$
$$K_5 = p_{NO}^2 / p_{N_2} p_{O_2} \quad (11)$$
$$K_6 = p_H^2 / p_{H_2} \quad (12)$$
$$K_7 = p_O^2 / p_{O_2} \quad (13)$$
$$K_8 = p_N^2 / p_{N_2} \quad (14)$$
$$K_9 = p_H p_{Cl} / p_{HCl} \quad (15)$$

Based on the dissociation reaction

$$H_2S \rightleftharpoons H_2 + S(凝)^{(1)}$$

Key: 1. Condensed

Therefore

$$K_{16} = p_{H_2} / p_{H_2S} \quad (16)$$
$$K_{18} = p_{Cl}^2 / p_{Cl_2} \quad (17)$$

Based on the Dalton Law

$$p_C = p_\Sigma = \Sigma p_i \quad (18)$$

Among the 18 above designed equations, because only two of equations (7), (8) and (9) are independent, therefore the equilibrium composition system of equations only have 17 independent equations. The unknown number is also only 17 (the

total pressure p_{Σ} of the combustion product and the partial pressure of 16 types of compositions). Based on mathematical theory, this system of equations is understandable.

III. Simplified Method of a System of Equations

From equations (5)/(4), we obtain

$$\frac{Cl_r}{N_r}=\frac{35.45}{14}\ \frac{p_{HCl}+2p_{Cl_2}+p_{Cl}}{2p_{N_2}+p_{NO}+p_N}$$

Then

$$\frac{p_{HCl}+2p_{Cl_2}+p_{Cl}}{2p_{N_2}+p_{NO}+p_N}=\frac{14}{35.45}\ \frac{Cl_r}{N_r}=U=\text{const} \tag{19}$$

$$\therefore \quad UC=p_{HCl}+L \tag{20}$$

In the formula

$$C=2p_{N_2}+p_{NO}+p_N=2p_{N_2}+A \tag{21}$$

$$A=p_{NO}+p_N \tag{22 a}$$

$$L=2p_{Cl_2}+p_{Cl} \tag{22 b}$$

Therefore

$$p_{HCl}=CU-L \tag{23}$$

From equations (6)/(4), we obtain

$$\frac{p_{SO_2}+p_{H_2S}}{C}=\frac{14}{32}\ \frac{S_r}{N_r}=V=\text{const} \tag{24}$$

Letting

$$F = p_{H_2S}$$

Therefore

$$p_{SO_2} = CV - F \tag{25}$$

From equations (1)/(4), we can obtain

$$\frac{p_{CO_2} + p_{CO}}{C} = \frac{7}{6}\ \frac{C_P}{N_P} = Q = \text{const} \tag{26}$$

Therefore

$$p_{CO_2} + p_{CO} = CQ = \Phi \tag{27}$$

Then we obtain

$$p_{CO} = \Phi - p_{CO_2} \tag{28}$$

From equations (3)/(1), letting

$$D = 2p_{O_2} + p_{NO} + p_{OH} + p_O \tag{29}$$

we can obtain

$$\frac{2p_{CO_2} + p_{CO} + p_{H_2O} + 2p_{SO_2} + D}{p_{CO_2} + p_{CO}} = \frac{3}{4}\ \frac{O_P}{C_P} = S = \text{const} \tag{30}$$

$$p_{CO_2} + (p_{CO_2} + p_{CO}) + p_{H_2O} + D + 2p_{SO_2} = S\,(p_{CO_2} + p_{CO})$$

$$p_{CO_2} + p_{H_2O} + D = (S - 1)(p_{CO_2} + p_{CO}) - 2p_{SO_2}$$

After $(P_{CO_2}+P_{CO})$ is replaced by equation (27) and P_{SO_2} is replaced by equation (25), the above equation changes to

$$p_{CO_2}+p_{H_2O}+D=(S-1)CQ-2CV+2F$$

Therefore

$$p_{H_2O}=C[Q(S-1)-2V]-D+2F-p_{CO_2}$$

That is, we obtain

$$p_{H_2O}=X-p_{CO_2} \qquad (31)$$

In the formula

$$X=C\alpha-D+2F \qquad (32)$$

$$\alpha=Q(S-1)-2V=\text{const} \qquad (33)$$

From equations (2)/(4), we obtain

$$\frac{2p_{H_2O}+2p_{H_2}+p_{HCl}+B}{C}=14\frac{H_P}{N_P}=R=\text{const} \qquad (34)$$

In the formula:

$$B=p_{OH}+p_H+2p_{H_2S}=p_{OH}+p_H+2F \qquad (35)$$

$$2p_{H_2O}+2p_{H_2}+p_{HCl}+B=CR$$

Then

$$2(p_{H_2O}+p_{H_2})=CR-p_{HCl}-B \qquad (36)$$

When the P_{HCl} is replaced by equation (23), equation (36) changes to

$$2(p_{H_2O}+p_{H_2})=CR-CU+L-B$$

$$p_{H_2}=\frac{1}{2}[C(R-U)+L-B]-p_{H_2O}$$

When the P_{H_2O} is replaced by equations (31), (32) and (33)

$$p_{H_2}=\frac{1}{2}[C(R-U)+L-B]-[C\alpha-D+2F-p_{CO_2}]$$

$$p_{H_2}=C\left[\frac{1}{2}(R-U)-\alpha\right]+\frac{1}{2}(L-B)+D-2F+p_{CO_2}$$

That is, we obtain

$$p_{H_2}=\Psi+p_{CO_2} \qquad (37)$$

In the equation

$$\Psi=C\beta+\frac{1}{2}(L-B)+D-2F \qquad (38)$$

$$\beta=\frac{1}{2}(R-U)-\alpha=\text{const} \qquad (39)$$

When equations (28), (31) and (37) are substituted into equation (9)

$$K_p=(\Phi-p_{CO_2})(X-p_{CO_2})/p_{CO_2}(\Psi+p_{CO_2})$$

After the above equation is expanded and simplified, we can obtain

$$(K_p-1)p^2_{CO_2}+(\Phi+X+\Psi K_p)p_{CO_2}-\Phi X=0 \qquad (40)$$

Equation (40) is the control equation for controlling the major composition's partial pressure P_{CO_2}. A positive root of equation (40), that is P_{CO_2}, is separately substituted into equations (28), (31) and (37) and so we find the values of P_{CO}, P_{H_2O} and P_{H_2}.

2. The P_{N_2} Formula

The calculation factors Φ, X and Ψ in equation (40) all contain factor C and $C=2_{PN_2}+A$. Therefore, before solving equation (40) we must first find the value of PN_2.

Based on equation (18)

$$p_C = p_{CO_2} + p_{CO} + p_{H_2O} + p_{H_2} + p_{N_2} + p_{HCl} + p_{SO_2} + E \qquad (41)$$

In the formula:

$$E = p_{O_2} + p_{OH} + p_{NO} + p_{H_2S} + p_{Cl_2} + p_O + p_{Cl} + p_N + p_H \qquad (42)$$

From equation (36) we obtain

$$2(p_{H_2O} + p_{H_2} + p_{HCl}) = CR + p_{HCl} - B$$

After the P_{HCl} on the right side of the above equation is replaced by equation (23), it then changes to

$$p_{H_2O} + p_{H_2} + p_{HCl} = \frac{1}{2}C(R+U) - \frac{1}{2}(B+L) \qquad (43)$$

The P_{SO_2} in equation (41) is replaced by equation (25), the $(P_{CO_2} + P_{CO})$ is replaced by equation (27) and at the same time substituted into equation (43). After merging we can obtain

$$p_C = C\gamma + E - \frac{1}{2}(B+L) + p_{N_2}$$

In the formula

$$\gamma = \frac{1}{2}(R+U) + Q + V = \text{const} \qquad (44)$$

Therefore

$$p_C = (2p_{N_2} + A)\gamma + E - \frac{1}{2}(B+L) + p_{N_2}$$

Then we obtain

$$p_{N_2}=\frac{p_C+(B+L)/2-A\gamma-E}{2\gamma+1} \tag{45}$$

3. Iterative Calculation Method for Equilibrium Compositions

The above derived formulae are arranged into two systems of equations

$$\left.\begin{aligned}
p_{N_2}&=\left[p_C+\frac{1}{2}(B+L)-A\gamma-E\right]/(2\gamma+1)\\
p_{CO_2}&=\{-(\Phi+X+\Psi K_p)+[(\Phi+X+\Psi K_p)^2\\
&\quad+4(K_p-1)\Phi X]^{0.5}\}/2(K_p-1)\\
p_{CO}&=\Phi-p_{CO_2}\\
p_{H_2O}&=X-p_{CO_2}\\
p_{H_2}&=\Psi+p_{CO_2}\\
p_{SO_2}&=CV-F\\
p_{HCl}&=CU-L
\end{aligned}\right\} \tag{46}$$

The set of equations in (46) are equations for the partial pressure of seven major types of compositions of combustion products.

We can calculate the set of equations for the partial pressure of nine secondary compositions from equations (7), (10) and (11)-(17).

$$\left.\begin{aligned}
p_{O_2}&=(K_1p_{CO_2}/p_{CO})^2\\
p_{OH}&=K_3p_{H_2O}/p_{H_2}^{0.5}\\
p_{NO}&=(K_4p_{N_2}p_{O_2})^{0.5}\\
p_H&=(K_5p_{H_2})^{0.5}\\
p_O&=(K_6p_{O_2})^{0.5}\\
p_N&=(K_7p_{N_2})^{0.5}\\
p_{Cl}&=K_9p_{HCl}/p_H\\
p_{H_2S}&=p_{H_2}/K_9\\
p_{Cl_2}&=p_{Cl}^2/K_{10}
\end{aligned}\right\} \tag{47}$$

The iterative calculation procedure is as follows: assuming the partial pressure of the 9 types of secondary compositions is zero, we can then use the set of equations in (46) to directly find the first degree approximation of the partial pressure of 7 types of major compositions. This value is substituted into the set of equations in (47) to find the second degree of approximation of the partial pressure of 9 types of secondary compositions. Then, we use (46) to calculate the partial pressure of the major compositions. This iterative procedure is continuously carried out until the calculation results converge to the required accuracy.

The iterative convergent conditions vary with the required accuracy. If accuracy requirements are high, the convergent conditions are

$$\left.\begin{aligned} p_i^{(n+1)} - p_i^{(n)} &\leqslant 5 \times 10^{-4}\,\text{atm}\,(p_i > 1\ \text{atm}) \\ p_i^{(n+1)} - p_i^{(n)} &\leqslant 5 \times 10^{-5}\,\text{atm}\,(p_i < 1\ \text{atm}) \end{aligned}\right\} \qquad (48)$$

If the accuracy requirements for the partial pressure are not very high, the convergent conditions can appropriately widen.

4. Check Formula

When the two sides of equations (27), (32) and (38) are increased, after arrangement we obtain

$$\Phi + X + \Psi = CQ + \frac{1}{2}CR - \frac{1}{2}CU + \frac{L}{2} - \frac{B}{2}$$

The CQ on the right side of the above equation is replaced by equation (27), the CU is replaced by equation (23), the CR is replaced by equation (36) and after merging and arrangement, we obtain

$$\Phi + X + \Psi = p_C - (p_{N_2} + p_{HCl} + p_{SO_2} + E) \qquad (49)$$

Before solving the control equation, we must use equation (49) to check as to whether coefficients Φ , X and Ψ are correct, the value difference between the two sides of equation (49) is very small. Generally, it should be smaller than 1×10^{-3}atm (formed by the calculation accumulation errors).

The partial pressure values of P_{CO_2} , P_{CO} and PH_2 should be checked by equation (9) each time of iterative calculation. The partial pressure of the entire composition should be checked by equation (18). The final results of the partial pressure of each type of composition must be checked by mass conservation equations (1)-(6).

IV. Calculation Examples

Example: the hypothetical chemical formula of a certain known trademark polysulfide propellant is

$$C_{11.6830}H_{38.4820}O_{23.9550}N_{6.2520}Cl_{6.1970}S_{2.2800}Al_{3.2977}Cr_{0.1688}Cu_{0.1688}$$

With combustion chamber pressure P_C =60 atm and combustion product temperature T_C =2900K we find the pressure of the equilibrium composition of the combustion product.

To compare the results obtained from this method and the concentration method [2], the very small amount of composition contained in the combustion product was disregarded, that is we assumed

$$p_{Cl_2}=p_{H_2S}=p_O=p_N=0$$

1. The Weight Component of the Propellant Element

$$C_P=0.14020,\ H_P=0.03848,\ O_P=0.38328$$
$$N_P=0.07353,\ Cl_P=0.18423,\ S_P=0.07296$$
$$Al_P=0.08897,\ Cr_P=0.00826,\ Cu_P=0.01009$$

Check: $\sum G_i=1.00000$

The oxygen Og kg required for producing the gas phase composition

$$O_g = O_p - O_{Al} - O_{Cr} = 0.38328 - 0.07914 - 0.00381 = 0.30033 \text{ kg}$$

2. Weight of the Condensed Phase and Gas Phase Composition in the Combustion Product

$$Y_s = M_{Al_2O_3} + M_{Cr_2O_3} + M_{Ca} = 0.16811 + 0.01207 + 0.01009 = 0.19027 \text{ kg}$$

$$Y_g = 1.0 - Y_s = 0.80973 \text{ kg}$$

3. Propellant's Component Constant and Constant Factor

$$Q = 2.22449, \quad R = 7.32653, \quad S = 1.60662, \quad U = 0.98948$$

$$V = 0.43411, \quad \alpha = 0.48120, \quad \beta = 2.68733$$

$$\gamma = 6.81661, \quad 2\gamma + 1 = 14.63322$$

4. Calculation of Partial Pressure of Gas Phase Equilibrium Composition

The calculation procedure is as shown in table 1.

(1)序号	计算式 (2) \ (3)迭代次数	p_i	1	2	3	4
1	$(K_1 p_{CO_2}/p_{CO})^2$	p_{O_2}	0	0.0000266	0.0000267	0.0000267
2	$K_3 p_{H_2O}/p_{H_2}^{0.5}$	p_{OH}	0	0.02422	0.02407	0.02408
3	$(K_4 p_{N_2} p_{O_2})^{0.5} = A$	p_{NO}	0	0.00112	0.00112	0.00112
4	$(K_5 p_{H_2})^{0.5}$	p_H	0	0.54247	0.53857	0.53859
5	$(K_6 p_{HCl}/p_H)$	p_C	0	0.13567	0.13357	0.13360
6	$B = p_{OH} + p_H$		0	0.56669	0.56264	0.56267
7	$D = 2p_{O_2} + p_{NO} + p_{OH}$		0	0.02540	0.02525	0.02526
8	$E = p_{O_2} + p_{OH} + p_{NO} + p_H + p_{Cl}$		0	0.70351	0.69736	0.69742

(4)序号	计算式 (5) \ (6)迭代次数	p_i	1	2	3	4
9	AY		0	0.00763	0.00763	0.00763
10	$(B + p_{Cl})/2$		0	0.35118	0.34811	0.34814
11	$p_C - E - AY + (B + p_{Cl})/2$		60	59.64004	59.64312	59.64309
12	$[p_C - E - AY + (B + p_{Cl})/2]/2Y + 1$	p_{N_2}	4.1003	4.0757	4.0759	4.0759
13	$C = 2p_{N_2} + A$		8.2006	8.1525	8.1529	8.1529
14	$\Phi = CQ$		18.2422	18.1352	18.1361	18.1361
15	CV	p_{SO_2}	3.5600	3.5390	3.5392	3.5392
16	$C\alpha$		3.9461	3.9230	3.9232	3.9232
17	$C\beta$		22.0377	21.9082	21.9093	21.9093
18	$CU - p_{Cl}$	p_{HCl}	8.1143	7.9312	7.9337	7.9337
19	$X = C\alpha - D$		3.9461	3.8976	3.8980	3.8979
20	$-(B - p_{Cl})/2$		0	-0.2155	-0.2145	-0.2145
21	$\Psi = C\beta + D - (B - p_{Cl})/2$		22.0377	21.7181	21.7201	21.7201
22	$\Phi + X + \Psi$(验算) (7)	(9)	44.2260	43.7509	43.7542	43.7541
23	$p_C - (E + p_{N_2} + p_{SO_2} + p_{HCl})$	验算	44.2254	43.7507	43.7538	43.7538
24	$\Psi K_p + \Phi + X$		180.9038	178.4466	178.4623	178.4622
25	$[\Psi K_p + \Phi + X]^2$		32726.1849	31843.1891	31848.7925	31848.7568
26	$4(K_p - 1)\Phi X$		1785.8163	1753.5237	1753.7896	1753.7446
27	$\{(\Psi K_p + \Phi + X)^2 + 4(K_p - 1)\Phi X\}^{0.5}$		185.7741	183.2941	183.3101	183.3099
28	$[㉗ - ㉔]/12.404$	p_{CO_2}	0.3926	0.3908	0.3908	0.3908
29	$\Phi - p_{CO_2}$	p_{H_2O}	17.8496	17.7444	17.7453	17.7453
30	$X - p_{CO_2}$	p_{H_2O}	3.5535	3.5068	3.5072	3.5071
31	$\Psi + p_{CO_2}$	p_{H_2}	22.4303	22.1089	22.1109	22.1109
32	$p_{CO} \cdot p_{H_2O}/p_{CO_2} \cdot p_{H_2}$(验算) (8)	K_p	7.2028	7.2019	7.2025	7.2023
33	$p_\Sigma = \Sigma p_i$	p_C	60.0006	60.0002	60.0004	60.0003

Table 1

Table 1 Calculation Procedure for the Partial Pressure of the Combustion Product (P_C=60 atm, T_C=2900K)

Key: 1. Number
2. Calculation formula
3. Number of times of Iteration
4. Number
5. Calculation formula
6. Number of times of iteration
7. Check
8. Check
9. Check

Mass conservation equations (1)-(6) are used to check the partial pressure of the fourth iterative calculation.

$\sum_{1}^{12} m_i p_i$=1256.9492, the checking results are listed in table 2.

(1) 重量组成 \ (2) 元素	C	H	O	N	Cl	S
(3) 推进剂	0.14020	0.03848	0.30033	0.07353	0.18423	0.07296
(4) 燃烧产物	0.14020	0.03848	0.30033	0.07353	0.18423	0.07296

Table 2

Key: 1. Weight component
2. Elemen t
3. Propellant
4. Combustion product

We can see from this that the calculations are totally correct.

V. Concluding Remarks

1. The Congruence of the Partial Pressure of Each Type of Composition

The major composition

$$\Delta p_{max} = p_{H_2O}^{(4)} - p_{H_2O}^{(3)} = 0.0001$$

Calculations showed that the congruence of the partial pressure of each type of composition is very good and completely agrees with the congruent conditions of equation (48). The congruent speed was also very fast and the fourth iteration exceeded the congruent accuracy.

2. Comparison With the Concentration Method

The combustion product compositions in this paper were indicated by pressure. The secondary composition formulae are those of (47). However, when the concentration method is indicated by the gram molecular number, then

$$n_{OH} = (K_3 n_{H_2O}/n_{H_2}^{0.5})(p_C/n_g)^{-0.5}$$

By comparing the above two formulae, we can see that when the composition is indicated by pressure, none of the calculation formulae have the exponential factor $(P_C/n_g)^{-\Delta\nu}$. Therefore, the formulae are simple and calculations are convenient.

Based on table 3 we know that the maximum corresponding error of the partial pressure is

$$\left[\frac{\Delta p_i}{p_i}\right]_{max} = \frac{\Delta p_{NO}}{p_{NO}} = 0.0024 = 0.24\%$$

Therefore, it is said that the results of the two methods are identical.

(1)分压 \ (2)方法	(3) 浓度法	(4) 本法	$\Delta p_i/p_i$	(5)分压 \ (6)方法	(7) 浓度法	(8) 本法	$\Delta p_i/p_i$
p_{O_2}	0.00031	0.00031	0	p_{HCl}	9.8910	9.8881	+0.0003
p_{OH}	0.07785	0.07777	+0.0010	p_{CO_2}	1.3798	1.3776	+0.0016
p_{NO}	0.00425	0.00424	+0.0024	p_{CO}	18.2931	18.2903	+0.0002
p_H	0.50853	0.50870	−0.0003	p_{H_2O}	10.7075	10.6996	+0.0007
p_{Cl}	0.17637	0.17630	+0.0004	p_{H_2}	19.7107	19.7243	−0.0007
p_{N_2}	5.0315	5.0301	+0.0003	Σp_i	70.0067	70.0003	
p_{SO_2}	4.2258	4.2230	+0.0007				

(9注：1．按文献[2]推进剂数据计算；2．浓度法计算得到的成分的克分子数，按公式：$p_i = p_c n_i/n_g$换算成压力；3．两种方法都是4次迭代结果。

Table 3 Comparison of the Calculation Results of This Method and the Concentration Method (P_C=70 atm, T_C=2900K)

Key: 1. Partial pressure
2. Method
3. Concentration method
4. This method
5. Partial pressure
6. Method
7. Concentration method
8. This method
9. Notes: 1. Propellant data calculations based on reference [2];
2. Composition's gram molecular number from calculations by concentration method: $p_i=p_c n_i/n_g$ conversion into pressure;
3. Both methods have the results of four times of iteration.

3. This method is also suitable for other types of propellants, especially for double-base propellants.

References

[1] Fundamental Problems of Solid Propellant Rocket Engines (Vol.1); F.A. Williams, author, Jing Guchun, tr., National Defense Publications, (1976).

[2] The Design of Solid Rocket Engines (Vol.1), Peking College of Aeronautics, (1976).

[3] The Energy Characteristics of Chemical Propellants, I. Glasman et al, Li Hongyao, tr. National Defense Publications, (1979).

A COMMENT ON THE PLATEAU COMBUSTION MECHANISM OF DOUBLE-BASE PROPELLANTS

by Ma Xieqi

Abstract

This is a comment using 58 references on the plateau combustion mechanism of double-base propellants. The experiments, evidences and view points for each principle are briefly presented, analyzed and reviewed. Views concerning future work are brought forth.

I. Preface

The burning rate of plateau double-base propellants in a certain pressure range appears to be unrelated to pressure. This is very advantageous for rocket engine work. For this reason, a large number of scientific research personnel have attempted to clarify the plateau combustion mechanism so as to better control, utilize and develop plateau propellants. This paper will briefly analyze and comment on the various view points, evidences and experiments related to the plateau combustion mechanism of double-base propellants.

II. The Subsurface Condensed Phase Theory

Camp et al [1] (1958) pointed out that after a lead compound is added into a double-base propellant, the lead compound can absorb the ultraviolet rays emitted in the flame region. This changes the ester nitrate degraded photosensitizer. As a result, this accelerates the ester nitrate degradation, raises the burning rate of the propellant and produces super burning rate combustion. Yet, following the rise of the propellant's

burning rate, the vanishing speed of the condensed phase quickens, the effective operating time of the photochemical reaction in the subsurface reaction region shortens, the level of the super burning rate combustion drops and plateau combustion drops and plateau combustion is produced. When the pressure increases further, the condensed group produced by the lead compound obstructs the absorption by the subsurface of ultraviolet rays. This causes the burning rate to decrease and produces mesa combustion.

Camp et al [2] (1975) used a catalyst with different excitation modes radiated by ultraviolet light to develop the photochemical reaction theory. Experiments by Kubota et al [3] proved that increases in burning speed are related to the amount of light radiated from the outside but is unrelated to the amount of ultraviolet light. However, Camp considers that the photochemical reaction theory is still effective for producing certain catalysts with high pressure plateaus. Under low pressure, catalytic combustion has an unluminous flame yet lead compounds can still increase the propellant's burning rate. Therefore, at least under low pressure, the super burning rate combustion is unrelated to the photochemical theory.

2. The Chemical Equivalent Shift Theory

Kubota et al [3,4] (1973) used high-speed photography and fine thermocouples to research the reactions of combustion waves in each region. Lead salt causes the combustion surface to accumulate carbon bearing substances and the corresponding burning rate also increases. However, the lead salt does not change the amount of heat released by the surface. It only causes the hissing region's thermal conduction feedback to increase 50-100%. They consider that the appearance of carbon is the result of the ester nitrate decomposition producing changes and the decrease in the produced quantity of aldehyde. This causes the ratio of aldehyde and NO_2 to become even closer

to a chemical equivalent. However, the reaction of aldehyde and NO_2 is fastest under a chemical equivalent. As a result, this increased the reaction heat and raised the burning rate. Following the raising of the pressure, the effective time of the catalytic effect shortened, the quantity of aldehyde increased, the ratio of aldehyde and NO_2 departed from the chemical equivalent and the aldehyde and NO_2 reaction speed lowered which produced plateau combustion. Kubota also set up a mathematical model.This theory employed the research results of Pollard et al [5] on the propagation speed of the formaldehyde and NO_2 combustion flame. When the CH_2O/NO_2 ratio is 1/1.4, the burning rate is maximum. Its reaction is as follows:

This theory does not concretely explain how the lead compound changes the path of ester nitrate decomposition. It can only explain super burning rate combustion and plateau combustion but cannot explain mesa combustion. In actual propellant combustion, the changes of the chemical equivalent have a very large influence on the combustion process. We still await test proof. The reason for the production of super burning rate combustion and plateau combustion is the changes in the course of ester nitrate decomposition. It is produced in the condensed phase and is therefore listed in the condensed phase theory. Yet the action results occur in the gas phase's hissing region and thus can also be viewed as the condensed phase - gas phase theory.

3. The Chelate Theory

Suh and Lenchitz et al [6] (1974) used detonation tests and at the same time determined the gas product's composition method to discover the 50% decrease of NO in the combustion products of the catalytic propellant, the total amount of non-changing CO_2 and CO and the CO_2/CO ratio which actually slightly decreased. Simultaneously, they also discovered that the detonation heat of the catalytic propellant rose under low temperature and the

combustion surface temperature also rose. This paper considers that this was the result of the increase of the NO reduction quantity in the area of the surface. They proposed that the lead salt's lead atoms and the oxygen atoms of the ester nitrate form a chelate type compound and the electrons on the ester nitrate shift toward the divalent lead. This causes the $RO-NO_2$ chain to weaken and the ester nitrate decomposition quickens causing the burning rate to increase.

Early, in 1966, Lenchitz et al [7,8] researched the catalytic action mechanism. At the time, the ratio of the measured catalytic propellant 's combustion product CO_2/CO increased. This theory explained that the reason why the covalent compound of tetraphenyl lead does not have catalytic action is because it cannot form a chelate. Yet, it cannot explain lead tetraethyl, lead oxide and lead powder being able to cause double-base propellants to produce plateau combustion [9]. There is no direct evidence that the chelate accelerates the decomposition of the ester nitrate so that the detonation heat increase, when surface temperature rises and pressure is low, can also result in even more NO being reduced. Reference [10] considers that the reason the double-base propellant's detonation heat drops when there is low pressure is the expansion of the pressurized inert gas. The additional nickel powder causes the detonation heat to greatly increase under low pressure and also causes the luminous flame to be close to the combustion surface. The nickel powder, however, does not have a plateau reaction.

4. Spectral Method Research on the Action Position and Mechanism of Catalysts

Dr. Mal'tsev [11] (1973) showed in research using an ultraviolet transmitted spectrum that the catalytic combustion product CuH in the area of the double-base propellant's combustion surface with added copper salicylate had strong absorption, the

dark region was relatively narrow, the N_2O dissolving was very fast and the surface temperature rose. The copper compound caused the CO and CO_2 to appear even earlier possibly delaying the appearance of H_2O. This explains the accelerated gas phase reaction and thermal feedback toward the surface. However, the lead salicylate, the temperature along the flame's tongues of fire direction and the composition had no noticeable changes. The lead spectral line was not included. This also explains that the lead salacylate greatly accelerated the chemical decomposition of the initial condensed phase of the combustion as well as the action of the solid phase transforming into a gas phase. The lead caused the H_2O to appear even earlier, to obtain carbon bearing substances and then to be burned off.

Based on the spectrum, they proved that the lead acted in the condensed phase, the copper acted in the gas phase and the two acted independently in different combustion regions. Yet, the later mentioned Androsov et al considered that the increased effect on the lead was a type of non-added effect. Baer et al [12] of the United States also confirmed Mal'tsev's results. Because the experiments were carried out in actual combustion systems, they were more believable. Yet, the combustion surface was full of bumps and hollows and it was very difficult to differentiate within a several micrometer to several ten micrometer space on the surface. Therefore, it was necessary to raise the resolution and use a low plateau pressure propellant in order to be able to further show the chemical catalytic nature.

5. Heat Decomposition-Gas Phase Chromatographic Research Results

The Androsov Research Group used heat decomposition-gas phase chromatography as the basic method to systematically study the action mechanism of lead-copper propellants. On the one hand, they researched the characteristics of the lead-copper

composite catalysis such as the influences of initial temperature and pressure [13], the influence of the propellant component [14], the influences of the lead-copper ratio [15] etc. in order to obtain perceptual knowledge. On the other hand, they used heat decomposition chromatography to find chemical evidence [16,17,18], to test and verify the obtained perceptual knowledge and to gain rational knowledge. In 1978, they published "The Mechanism of Lead-Copper Composite Catalysts on Propellant Combustion Action."

Their research showed that CuO does not change the decomposition speed of ester nitrate but causes the amount of CO in the combustion product to decrease, the amount of CO_2 to increase and the CO to oxidize into CO_2. When the cellulose nitrate decomposes, it is necessary to have the participation of CuO and when the glycerine nitrate decomposes, it is necessary to have the participation of NO_2. The action of the lead oxide causes the highest quantity of heat of the CO_2 product in the decomposed product to increase. It also causes the reaction ability ratio of NO and NO_2 when in combustion to increase the quantity of the high N_2O. As a result, super burning rate combustion is produced. The increase in strength of the lead-copper catalytic action (exceeds the total independent action of the two) is owing to the PbO causing the CO_2 and N_2O to increase and the CO to decrease in the propellant's decomposed products. Because the decrease of CO is beneficial to the catalytic action of CuO, this causes even more CO to transform into CO_2.

The increase of glycerine nitrate in the propellant causes the action of the CuO to drastically drop and when the glycerine nitrate exceeds 40%, the action completely disappears. This is because the CO formed when the glycerine nitrate decomposes is much greater than the CO_2 and the surface of CuO sustains CO poisoning. When double-base propellants with 52% of diethyl glycol ester dinitrate is at above 40 atm pressure, the action

of CuO is stronger than the action of PbO_2 and if a lead-copper composite catalyst is used, the catalytic effect is greatly increased. Yet, when in 70-100 atm pressure, mesa combustion is produced. Diethyl glycol ester dinitrate decomposition releases a great deal of N_2O and produces CO. However, the N_2O causes the burning rate to increase and the CO causes CuO poisoning. This indirectly verified the action mechanism of the lead-copper composite catalyst. They employed common procedures to rather fully explain the chemical qualities of the production of the super burning rate and plateau and mesa combustion. Because the heat decomposition and combustion processes are linked as well as have differences, we will await other direct test verification.

6. Mass Spectra Research Results

Bauman [20] (1965) and Dauerman [21,22] (1968) first used mass spectra to research the effects of catalysts on double-base propellant heat decomposition. Faber [23] (1976) used a specially designed four differential pump mass spectrometer to study the products formed in combustion flames under constant pressure. After the nozzle dropped in pressure many times the speed dropped to 10^{-9} atm pressure and this molecular beam entered the mass spectrometer for analysis. It was discovered that when lead-copper oxyacid salts decompose, metallic lead and copper are produced but the non-catalytic action of manganese salt produces MnO. The covalent linked tetraphenyl lead vaporizes but does not decompose. The gaseous lead and copper atoms react with the ester nitrate and produce $PbNO_2$ and $CuNO_2$. These compounds are stable under suitable temperatures. When the nitrite enters into combustion area, a reaction occurs which produces hydrogen oxides and oxides. This is consistent with thermal dynamic prediction. Therefore, the appearance of $PbNO_2$ and $CuNO_2$ is possibly the differentiating standard of plateau combustion.

This research maintains the view that when the ester nitrate decomposes, the CO-NO_2 separates into CO and NO_2 which does not verify the NO_3 discovered by Bauman and Dauerman. It does not coincide with Prekel's Pb-PbO cycle oxidation reduction reaction but is identical to Suh's hypothesis. That is, the NO_2 uses a certain method and the lead action in the lead salt yet does not form a chelate. It does, however, form $PbNO_2$. The gas state Pb and NO_2 reaction can cause the ester nitrate to release even more NO_2 and thus increase the burning rate. Mass spectra is a powerful tool for studying condensed phase reactions. If the system proposed by White [25] is used for study under high pressure, the molecular beam will instantly be sent into the mass spectra and this will make an important contribution for the plateau catalytic mechanism.

7. Results of Differential Scanning Calorimetric Tests

Eisenreich et al [26,27] (1976) used a differential scanning calorimeter to simultaneously carry out heat weightlessness and heat analysis tests. It was proven that the first step of double-base propellant heat decomposition is glycerine nitrate vaporization and the second step is the heat decomposition of the cellulose nitrate. Under low pressure, the reaction heat of the catalytic propellant must be higher than that for non-catalysis. Its law is identical to Lenchitz's determinations using the detonation heat method [8,9]. The peak temperature of catalytic propellant decomposition is relatively high and active energy is relatively low. Similar work done domestically has also obtained the same law.

Eisenreich et al [28] (1978) continued to research the influence of copper and lead compounds on cellulose nitrate decomposition. Beatriz et al [29] (1978) then used a differential scanning calorimeter to find the major gas phase or multiphase reaction actions of double-base propellant trajectory modifiers on adjacent combustion surfaces. The heat quantity

measured by the differential scanning calorimeter is not pure solid reaction heat [30,31,32]. However, Eisenreich considered the solid phase reaction as essential and the catalyst as primarily acting in the solid phase. Differential scanning calorimetry is a modern heat analysis method which is quite effective for researching propellant heat decomposition. Although its heating speed differs greatly from the heating speed of real propellants, yet its results still have reference value. The recently developed heat analysis method which uses a high heating speed (100-20,000 degrees/second) is employed to study the ignition dynamics of propellants and explosives [33,34,35].

8. Measuring the Detonation Point and Finding the Activation Energy

Bai Mulan et al (1978) used the method of measuring the detonation point to find the reaction's activation energy and index forward factor. Under 200-250°C temperature, a 0.03 gram propellant sample is used to measure the explosion delay period under 6 temperatures. When making the $\ln\tau = \frac{E}{RT} + \ln C$ curve, we find E and C listed in the table as follows (in the formula: τ is the delay period, E is the activation energy, R is the gas constant and C is index forward factor):

(1)计算结果 \ 推进剂(2)	(5)硝化纤维素(Ⅰ)	(6) Ⅰ加2.6%苯二甲酸铅	(7) Ⅰ加2.6%碳酸铅	(8)某双基推进剂(Ⅱ)	(9) Ⅱ加2.6%苯二甲酸铅	(10) Ⅱ加2.6%碳酸铅
(3)活化能E(千卡/克分子)	24.40	23.41	21.40	18.46	16.54	16.02
(4)指前因数C(1/秒)	9.4×10^{8}	8.55×10^{8}	3.84×10^{8}	1.37×10^{7}	1.84×10^{6}	6.34×10^{5}

Key: 1. Calculation results
2. Propellant
3. Activation energy E (kilocalories/gram molecules)
4. Index forward factor C (1/second)

Key: 5. Cellulose nitrate (I)
6. I with 2.6% lead benzoate
7. I with 2.6% lead tannate
8. A certain double-base propellant (II)
9. II with 2.6% lead benzoate
10. II with 2.6% lead tannate

It can be seen from the data listed in the table that the catalyst causes the double-base propellant and cellulose nitrate activation energy to decline, the condensed phase reaction to accelerate and the burning rate to increase.

The activation energy measured by this method is naturally the explosion reduction period's activation energy which is different from the concept of explosion reaction or combustion reaction activation energy. If there is identical control of the reaction, the activation energy will also be the same. Zenin [36] proposed a model for the double-base propellant's condensed phase reaction layer. He proved that the activation energy of ester nitrate decomposition is about 48-50 kilocalories / gram molecule and the combustion activation energy is 19 kilocalories/gram molecule activation energy of the NO_2 oxidized hydrocarbon. Therefore, the control reaction of double-base propellant combustion is possibly the oxidation reaction of NO_2. The activation energy measured by the detonation point method is basically the same as the combustion activation energy. It is very possibly the same as the control reaction, that is, the oxidation reaction of NO_2. The reaction when measuring the detonation point is not a pure solid phase reaction but should include the gas phase reaction of the solid phase surface. This can use simple test proof.

9. Another Result in Measuring the Surface Temperature

Denisyuk . et al [18] (1971) used a thermal couple to measure the temperature distribution curve of catalytic and non-catalytic H type explosives under 20-90 atm pressure. Moreover, they derived data on the surface temperature, thickness of the

stack gas area, the highest flame temperature, the distance from the surface to the highest flame temperature, the heat released by the condensed phase, the heat released by the stack gas area and the temperature gradient in the vicinity of the surface. They discovered that the catalyst did not change the distance from the surface to the highest flame so that the gas phase heat transfer decreased 4-5% and the stack gas area's heat loss also decreased. Therefore, the catalyst must act in the condensed phase to cause the burning rate to increase. Under high pressure, the gas product's solubility rises in the condensed phase which causes catalytic poisoning or the catalyst to become an inhibitor. As a result, the burning rate drops producing plateau and mesa combustion.

I used the thermal couple to measure the temperature so as to prove that catalysis occurs in the condensed phase, yet I do not know the concrete chemico-physical process. Under high pressure, it is difficult to measure the surface temperature correctly. The fact that the catalyst does not change the distance from the surface to the highest flame is opposite of Kuboto's measurement results mentioned in section 2.

III. The Gas Phase Theory

1. The Lead-Lead Oxide Cycle Theory

Steiberger [1] (1952) added organic lead salt into a propellant after decomposing it in a furnace and discovered that the catalytic effects were better. When in 350°C, the heat decomposed product was lead or lead oxide. They should be the cause of the propellant's plateau combustion. The organic part of the lead salt only acted to produce fine metallic lead or lead oxide. For this reason, he proposed the gas phase catalytic mechanism:

$$Pb + NO_2(NO) \longrightarrow PbO$$
$$PbO + CO(CH_2O,\ H_2,\ C_m) \longrightarrow Pb$$

Prekel [37] (1961) used a sealed exploder to measure the burning rate. He observed a broken piece of carbon fall down in the plateau pressure range and there was a melted lead ball. This phenomenon did not occur above the plateau pressure. He considered that the above mentioned reaction occured in the gas phase area or foam area. Preckel [38] (1965) also explained, based on the Pb-PbO cycle theory, that inorganic lead compounds and aliphatic lead compounds can only cause a low heat value catalyst to produce plateau combustion. However, aromatic compounds can cause a high heat value catalyst to produce plateau combustion.

This theory is quite rough. The lead-lead oxide cycle reaction is indirectly infered and is not directly evidenced. Preckel indicated the area of catalytic action and discovered that the broken piece of carbon was related to plateau combustion. This opened avenues for the lead and lead containing substances theory.

2. The Free Base Theory

Sinha et al [39] (1968) consider that the burning rate of double-base propellants is determined by the extinction speed and the extinction speed sustains the control of the hissing region on the surface heat transfer but is not influenced by the flame area. They adopted the test results of Paneth et al regarding the ability of lead to react with a free base at 400^{o}C to produce lead alkyl and the ability of lead alkyl to decompose at 600^{o}C into lead and a free base. The lead and ester nitrate decomposed free base combine in the foam area to form lead alkyl and in the hissing area the lead alkyl decomposes into a free base and lead. The free base produces a chain reaction which causes NO reduction, emits a large amount of heat, accelerates the transfer heat from the hissing area towards the foam area, causes the burning rate to rise and produces super burning rate combustion. However, for the non-catalytic propellant, the NO does not participate in the

reaction of the hissing area. When the pressure rises, the free base concentration in the hissing area rises and the free base automatically stops the collision increase which decreased the reaction between the free base and NO and lowers the transfer heat from the hissing area to the foam area. On the other hand, when the pressure rises, the heat induction coefficient of the gas increases and the heat transfer increases from the hissing area towards the foam area. In a certain pressure range, these two opposite effects are equal and this produces plateau combustion.

The free base theory of cellulose nitrate decomposition was proposed early by Wolfram et al [40]. Morrow [41] (1976) used a heat platform polarizing microscope to observe the liquefaction decomposition process of the pure cellulose nitrate and modified cellulose nitrate (adding a free base inhibitor, accelerating agent, burning rate catalyst and additive) when heated to 225^{o}C. Test results showed the occurence of an important free base process. This theory did not study the free base process in actual propellant combustion and thus cannot explain the mesa effect. Moreover, a large number of non-lead metals possibly react with the free base and produce alkyl metal free base yet there is no plateau combustion.

3. The Carbon Bearing Substance - Hot Light Sphere Theory

Eisenreich et al [42] (1978) used micro-high speed photography and a scanning electron microscope to observe the color of the solid phase area 40 micrometers below the combustion flame-out surface change from a certain transparency to a brown or brownish red color. They discovered that the largest diameter was a hollow of 50 micrometers and carbon covered the entire flame-out surface. The carbon particles had 20-50 micrometer coarse branches and the largest diameter was a 100 micrometer flat plate. The carbon particles were porous and the diameter of the holes were about 5 micrometers. When the carbon particles were above 5

atmospheric pressure there began to appear a red light which seemed to be the result of being oxidized by the decomposed products flowing by. At the same time, the carbon particles changed little, they flew from the surface and their number decreased. The diameters of the carbon particles in the plateau pressure range were about 20-50 micrometers and density was 300 particles/centimeter^2. When the pressure exceeded 5 atmospheric pressure, metallic light spheres appear on the carbon particles or combustion surface. The diameter is about 100 micrometers, the light spheres which flew from the surface have diameters of about 20-50 micrometers and their speed is 15-50 centimeters/second. They consider that the trajectory modifier accelerates the decomposition of cellulose nitrate below the combustion surface when under low pressure and catalyzes the oxidation of carbon bearing substances on the combustion surface. As a result, a great deal of energy is released and super burning rate combustion is produced. Because the carbon bearing and metal bearing light spheres leave the combustion surface and cause the energy conducted to the surface to diminish, plateau and mesa combustion are produced.

Early, in 1956, when Brown et al [1] used micro-high speed photography to observe the structure of the plateau propellant's combustion surface they discovered that under plateau pressure there are 30-60 micrometer diameter lead spheres. In the last several years, a good deal of domestic research work has confirmed the carbon bearing substance - hot light sphere theory. It can directly describe the forms, sizes, number and movements of the carbon bearing substances and metallic light spheres related to the production of plateau combustion. Although its chemical properties have not yet been precisely proven, yet its possible mechanism has been suggested. Reactions on the carbon particles have confirmed that the carbon-lead catalysis mentioned below produces a mechanism of super burning rate combustion.

4. The Lead-Carbon Catalysis Theory

Hewken et al [43] (1971) published a summary of the work of their research team. They used a flame probe to measure the composition of each combustion area, used a heat couple and the infrared heat measuring method to measure the temperature of the combustion surface and used high speed photography to study the structure of the combustion waves. They discovered that under low pressure, the introduction of a lead compound caused the temperature near the surface to rise; analysis of the catalytic propellant's dark area showed that the N_2 in the combustion products greatly increased and the NO decreased; there was a great amount of heat released from the NO reduction reaction; the action of the lead compound caused the combustion surface to produce a large amount of carbon. There was a great amount of carbon when in super burning rate combustion and there was carbon produced on the combustion surface within the whole pressure range yet the amount of carbon was much less under low temperature than the catalytic propellant. They considered that the action of the lead compound not only increased the production of carbon but also caused carbon activation. The activated carbon is the solid phase catalyst of the NO released heat reduction reaction and when there is a non-catalyst, the speed of the NO in the dark area reduction reaction is very slow. As a result, the heat of the combustion surface increases and the burning rate also increases. Yet, the lead oxidizes the NO and carbon reaction causing the carbon to disappear. When the pressure rises, the carbon disappears more easily, the NO reduction reaction slows down and the propellant's buring rate declines which produces mesa or plateau combustion.

Hewkin et al [44] (1974) continued research on the connection between combustion surface phenomena and the catalyst in order to prove the above mentioned theory. The observed copper compound had a slower carbon eliminating speed than the lead compound and therefore the catalysis maintained high pressure. When the lead

and copper acted simultaneously, the elimination of carbon was determined by the lead. By adding an oxygen rich substance of ammonium perchlorate or glycerine nitrate the carbon on the surface greatly decreased and the plateau effect was destroyed. The joining of the cellulose nitrate accelerated the production of carbon which caused the plateau effect to expand to even higher pressure. Hexogen does not change the flame structure. There is still a lead carbon covering yet the plateau effect is destroyed. This is possibly because the hexogen's decomposed product NO_2 causes catalyst poisoning. It explains that although the formation of carbon is important the reaction is also very fast [45] at 200°C and the simultaneous reaction of copper and lead is easier to carry out [46]. Therefore, the catalysis of the lead and copper themselves should be consiered the same as the carbon.

This theory can explain many phenomena. However, although the reaction of lead oxidizing NO and carbon consumes carbon the amount of released heat is very great and thus cannot offer a tenable argument. It appears that the use of Eisenreich's research can explain plateau combustion. That is, the carbon bearing and metal bearing light spheres leaving the surface cause the energy transmitted to the surface to diminish and produce plateau combustion.

5. The π Chain Complex Theory

Fifer et al [47] (1975) reported that when a laser ignited a thin film sample of cellulose nitrate and double-base propellant and it was burned under 1, 20 and 40 atm pressure, an infrared spectrum was used to measure the final product. Under super burning rate combustion pressure, a lead salt bearing propellant sample obtained an increase in the CO_2/CO ratio in the combustion product. This caused the surface and dark area temperatures to increase and the burning rate to increase. There was no noticeable effect of the water and NO_2 permeating

into the test sample on the combustion product. However, a small amount of O_2 catalyzed a reaction in which the CO oxidized into CO_2 and the NO reduced to N_2. They used Salooja's [48,49] (1967) π chain complex theory. That is, the PbO inhibits the hydrocarbon combustion yet forms a π chain surface complex with an oxygen bearing hydrocarbon derivative. This greatly accelerates the combustion of the oxygen bearing derivative. The special features of the catalytic reaction are that the amount of CO_2 produced increases, sometimes the amount of H_2 produced also increases, the PbO is reduced to Pb and the Pb is then oxidized into PbO. The PbO uses the same type of initial stage and quadratic solid phase decomposition reaction for the catalysis of the ester nitrate.

In his experiments, Fifer discovered that there was too little carbon which was not sufficient to cause a noticeable change in the NO_2/CH_2O ratio. As a result, he did not support Kubota's chemical equivalent shift theory. Their measured NO reduction quantity was very small and thus did not coincide with the large amount of NO being catalyzed by the reduced carbon-lead and the chelate theory. However, test results were based on measuring laser ignited thin film combustion products which even though differing from real propellant combustion were still worth studying.

6. Research Results of the Hot Platform Microscope

Morrow (1973-1974) used a hot platform microscope in researching thermal high molecular degradation as well as for a great deal of work in the areas of the condensed phase heat properties of cellulose nitrate with different degrees of nitrate and combustion propellants [50,51,52]. He specially researched the influence of catalysts on cellulose nitrate thin film combustion [53,54]. A 180 ± 40 micrometer thin film sample in a capillary melting point analyzer with an outer diameter of 1.5 millimeters was heated to $250^{\circ}C$, a polarizing microscope was used to observe the phenomena

during the heating process and the heat loss in weight was measured. Four sets of tests were carried out on inorganic and organic lead salicylate using 1 to 34 atm pressure and it was discovered that there was no great difference between the appearance, beginning bubble and ending bubble temperatures of the flower shaped substance. However, the amount of weight lost was opposite of the prediction and the loss of weight of the added catalyst was actually quite small. He considered that the catalyst does not act upon the solid phase reaction but only acts on the gas phase above the surface. This is identical to Hewkin's view. It appears that this type of method can only aid the procedure but cannot basically resolve the problem.

7. Other Evidence for the Gas Phase Theory

Lengellé et al [55] (1979) used the concept of a composite propellant's combustion mechanism to study the mechanism of a double-base propellant's plateau combustion. They synthesized their own test data with that of past references and proved that the surface temperature and combustion assumes a linear relationship and that the catalyst does not change this relationship. The condensed phase heat emission quantity calculated from the surface temperature greatly increases with the increase of the burning rate yet is not related to the catalyst. Therefore, the propellant's decomposition dynamics are not influenced by the catalyst, the decomposition's manifested activation energy is about 40 kilocalories/gram molecule and is possibly correlated with the CO-NO_2 chain breaking. When a porous metallic pyrolytic instrument was used to study the decomposition of propellants in a vacuum and its produced gas was determined by a mass spectrometer, it was discovered that the influence of the catalyst on the gas composition was not great. Further, as regards decomposition dynamics, the copper and lead salt has still not changed in the condensed phase. A conclusion is made from this that although the propellant releases a large amount of heat in the condensed phase the catalyst does not act upon the condensed

phase process. The active products PbO and CuO of the catalyst only act in the initial flame and therefore the precision properties and stability of the lead salt are not major factors. They used the reaction of PbO and formaldehyde in a simulation reactor (residence time was about 0.1 seconds, the temperature reached 350°C) to prove that this reaction very possibly produces carbon on the propellant's surface. They also discovered that the end temperature of the initial flame rises with the pressure and when there is super burning rate combustion the corresponding initial flame end temperature is even higher. Therefore, the action position of the catalyst is in the gas phase's initial flame area. When there is lead and copper salt, the PbO and formaldehyde reaction in the initial fame produces carbon dregs causing even more NO to participate in the reaction and thus releases more heat and produces super burning rate combustion.

A porous plate pyrolytic instrument was used to study the decomposed products which disappeared in the condensed phase when there was no gas phase reaction. When research was already done on propellants with no catalyst, then when there is a catalyst research should be continued. Evidence of gas phase catalysis is obtained indirectly and we still await research for direct evidence. The method of researching composite propellants is very useful and should be extended to many other items.

8. The Theory of the Reaction With No Relation Between the Hissing Area and Pressure

In order to obtain more accurate surface temperature and clearer photographs of each area of the flame, Kubota [56] (1979) used a specially developed formulation with low plateau pressure, a wide range and a low burning rate. This plateau propellant had very strong super burning rate combustion properties under 16 atm pressure and under 16-36 atm pressure the plateau burning rate was 0.24 centimeters/second. The corresponding non-catalytic propellant's pressure index was 0.85.

Research found that the dark areas total reaction progression was 2.6 which is unrelated to the existence of the catalyst. This shows that the catalyst does not change the process of the dark area. The burning rate does not change in the plateau area but increases with the pressure. The catalytic propellant's luminous flame area approaches the combustion surface faster than the non-catalytic propellant's luminous flame area. The temperature gradient of the non-catalytic propellant's hissing area uniformly rises with the pressure but the temperature gradient of the catalytic propellant's hissing area rises in the super burning rate region and does not change in the plateau region. The hissing area temperatures of the two types of propellants change with the pressure and are the same as the burning rate law of changing with the pressure. The temperature gradient of the catalytic propellant's hissing area remains invariant in the plateau region, that is, the reaction speed does not change. As a result, the feedback of the heat conducted from the hissing area to the combustion surface remains invariant in the entire plateau region. Nevertheless, the catalytic activity in the plateau area's hissing region is changing and moreover it rapidly decreases with the pressure increase. This is a result of the related inhibited reaction of the hissing area and the lead. The total reaction progression of Kubota [1] and the results of Suh [6] and Lengellé [55] but is identical to Denisyuk's results [18]. However, based on the observation of Denisyuk , the catalyst does not change the distance from the surface to the highest flame. This is opposite to Kubota's observations. Thus, Denisyuk obtained the condensed phase catalysis theory and Kubota obtained the gas phase's hissing area catalysis theory. Because of this, use of surface temperature and combustion area photographs to study the plateau catalyst's action mechanism still requires continued work. We can thus hope for uniformly recognized conclusions.

IV. Several Views on Future Research Directions

1. Research Objects

We should turn from simulated real combustion systems to real combustion systems. Here, real combustion systems point to real propellant formulations for combustion under high pressure but does not refer to combustion in real engines. To date, aside from high speed photography, surface temperature tests, discontinuing tests etc. on physical research methods and flame infrared emission spectrum, research has differed greatly with real propellant combustion conditions. In this way, only indirect, reference type data can be obtained so that definite conclusions cannot be made. Half the results are obtained with twice the effort and there is a good deal of waste. Therefore, in the future, tests which depart from real combustion conditions must be avoided. Naturally, relevant simulated tests are still indispensable supplementary measures.

2. Test Methods

Using the methods of high speed microphotography, heat couple heat measuring and observations of the flame-out surface, Eisenreich and Kubota have reached high levels in their research. They obtained a large number of active physical phenomena of the plateau effect and inferred the chemical properties of the plateau effect from the physical phenomena. For example, they inferred the possible chemical reactions from observation research on the carbon bearing substances, lead bearing substances and light spheres on the combustion surface. Further, they obtained the pressure index of each area and the chemical reaction progression and catalytic activity coefficient by measuring the temperature distribution and thickness of each area of combustion and carried out basic judgements for determining the plateau catalyst's action position and the chemical reaction types. This technique should be further improved. For example, raise the test accuracy, develop the measuring of the flame's gas phase temperature distribution and use color high speed photography. Flame-out surface research should also be changed from physical

phenomena to chemical components. There are some units in China which are expanding the use of electronic probes to research a propellant's flame-out surface.

Mass spectra are an important measure for studying condensed phase dynamics which should be given serious attention. The joint use of the molecular beam sampling technique and time jumping mass spectra can possibly be employed to study the instant products of flames under real combustion conditions. This is extremely useful for solving the plateau combustion mechanism. Naturally, there are still many difficult problems which must be overcome [25].

Laser holography and laser Raman spectrum are combustion examination techniques which await development [57,58]. Their advantage lies in examining real combustion systems under non-interference combustion conditions. Laser holographs can also measure flame temperature distribution and observe the combustion surface's physical structure, the catalysts etc. above the surface and the size, distribution and movement speed in the flame when existing in a flame. The laser Raman spectrum can measure the temperature of each point in the flame and the physical types and concentrations. Naturally, it is a superior examining technique for combustion chemical reactions. Among them, because the coherent anti-Stokes Raman scattering is very strong, can be locally analyzed and does not have fluorescent interference, it can be considered first for development.

3. Test Designs

Even if scientific and ingenious design tests use common test methods they can still obtain new and important conclusions. For example, Kubota designed a propellant for plateau combustion under 16-30 atm pressure wherein photography and temperature measuring accuracy were greatly increased and new reliable conclusions were obtained. Further, in order to verify the effect of the CH_2O and NO_2 reaction in the propellant, use of a

carefully designed formation can be envisioned for research. There are still bright prospects in the area of test designs.

4. Other Problems Related to Research and Plateau Combustion

For example: the effect of carbon on plateau and most double-base propellant combustion; the mechanism of ultraviolet light absorbers etc. raising the burning rate in the plateau area; the auxillary catalytic effect of copper on lead; the effect of inertial additives in double-base propellants; non-lead type plateau catalysts etc. These problems are all related to the plateau combustion mechanism.

To sum up, although the plateau combustion mechanism of double-base propellants has been researched by many scientists throughout the world for over 20 years, the various theories and explanations proposed still await truly substantial knowledge of this problem. Further, a large amount of research work still awaits us.

References

[1] Kubota, N., AD 763,786, 218PP, 1973.

[2] Singh, H., Rao, K.R.K., AIAA J., 15(11)1545-1549, 1977.

[3] Kubota, N. et al., Symp. (Intern.) Combust. 15th,529-537, 1975.

[4] Kubota, N. et al., AIAA J., 12(12)1709-1714, 1974.

[5] Poolard, F.H. et al., Trans. Fara. Soc., 46(328)281-289, 1950.

[6] Suh, N.P. et al., Combustion and Flame, 22(3)289-293,1974.

[7] Lenchitz, C. et al., AD 478,015, 1966.

[8] Lenchitz, C. et al., Combustion and Flame, 10(2)140-145, 1966.

[9] Preckel, R.F., USP 3, 033, 716, 6PP, 1962.

[10] Kimura Junichi, Hisao Tanami, "Industrial Gunpowder," 37(1)22-28, 1976.

[11] Mal'tsev, V.M. et al., F.G.V., 9(1), 133-139 (1973).

References

[12] Baer, A.D. et al., NASA-CR-140821, 1974.

[13] Denisyuk, A.P. et al, Trudy Moskva Khimiya-Tekhnologii Ins., 83, 114-118, 1974.

[14] Androsov, A.S. et al, F.G.V., 11(1), 18-26, 1975.

[15] Ibid, 12(5) 780-782, 1976.

[16] Ibid, 10(3), 338-341, 1974.

[17] Androsov, A.S. et al., Izvestiye VUZ Khimiya i Khimicheskaya Tekhnologiya, 19(8) 1191-1194, 1976.

[18] Denisyuk, A.P. et al., Izvestiye VUZ Khimiya i Khimicheskaya Tekhnologiya, 14(4), 861-864, 1971.

[19] Androsov, A.S. et al., F.G.V., 14(2) 63-66, 1978.

[20] Bauman, B.P. et al., AD 468, 333, 1965.

[21] Dauerman, S.K., AIAA J., 6(4) 668-673, 1968.

[22] Dauerman, S.K., AIAA J., 6(8), 1468-1473, 1968.

[23] Farber, M., ADA 035, 602, 1976.

[24] Farber, M., Combustion and Flame, 31(3)309-323, 1978.

[25] White, K.J. et al., ADA 013, 372, 32PP, 1975.

[26] Eisenreich, N. et al., Proceedings of the First European Symposium on Thermal Analysis, 452-453, 1977.

[27] Eisenreich, N. et al., Analysenmethoden Treib-Explosivst., Int. Jahrestag. Inst. Chem. Treib-Explosivest. Fraunhofer-Ges, 195-213, 1977.

[28] Eisenreich, N., Thermochimica Acta, 27(1-3)339-346, 1978.

[29] Beatriz, B.D.S., et al., Thermochimica Acta, 27(1-3) 347-356, 1978.

[30] Kirby, C.E., et al., AIAA J., 9(2)317-320, 1971.

[31] Thompson, C.L. et al., AIAA J., 9(1)154-159, 1971.

[32] Kirby, C.E., NASA Tech.Note, D-6105, 26PP, 1971.

[33] Beardell, A.J. et al., Thermochimica Acta, 14(1-2) 169-181, 1976.

References

[34] Petrick, J.T., Compat. Plast. Other Mater Explosive Propellants Pyrotech.Symp. IV-6, 6PP, 1976.

[35] Bouck, L.S., Chemical Abstruct, 76, 88007K, 1972.

[36] Zenin, A.P., DAN SSSR, 213 (6) 1357-60, 1973.

[37] Preckel, R.F., ARS J.31, 1286-1287, 1961, ARS Paper 61-1596, 10PP, 1961.

[38] Preckel, R.F., AIAA J. 3,346-347, 1965.

(39] Sinha, S.K. et al., Explosiv-stoffe, 10, 223-225, 1968.

[40] Wolfram, M.I. et al., Am. Chem.Soc., 77, P 6573, 1955.

[41] Morrow, S.I., Microscope. 24(3)227-235, 1976.

[42] Eisenreich, N. et al., Propellants and Explosives, 3(5)141-146, 1978.

[43] Hewkin, D.J. et al., Combustion Science and Technology, 2(5-6)307-327, 1971.

[44] Hewkin, D.J. et al., Verbrennugsvorgaenge Treib-Brennst., Jahrestag.Inst. Chem. Treib Explosivst. Franhofer-Ges, P.35-51, 1975.

[45] London, J.W., et al., J. Catalysis 31, P. 96-109, 1973.

[46] Sorensen, L.C. et al., Ind.Eng.Chem. Prod. Rev. Dev. (11)423-426, 1972.

[47] Fifer, R.A. et al., Combustion and Flame, 24(3)369-380,1975.

[48] Salloja, K.C., Combustion and Flame,11(1) P.247, 1967.

[49] Salloja, K.C., Combustion and Flame,11(6) 511-514, 1967.

[50] Morrow, S.I., Microscope, 22(4)349-359, 1974.

[51] Morrow, S.I., Anal. Calorimetry, 3, 757-775, 1974.

[52] Morrow, S.I., BRL, IMR 173, AMC Program, The Fundamentals of Ignition and Combustion, Vol. I, 1974.

[53] Morrow, S.I., Microscope, 22(4)341-348, 1974.

[54] Morrow, S.I., Microscope, 21(4)229-241, 1973.

[55] Lengellé, G. et al., Combustion (International) Symposium Combustion, 17th, 1443-1451, 1979.

[56] Kubota, N., Combustion (International)Symposium Combustion, 17th, 1435-1441, 1979.

[57] Briones, R.A. et al., Pros.Soc.Photo-Opt. Instrum. Eng., 125, 90-104, 1977.

[58] Goulard, R., Combustion Measurements, 1976.

END

FILMED

2-83

DTIC